Bull Eng Geol Environ (2015) 74:103–116
DOI 10.1007/s10064-014-0606-8

ORIGINAL PAPER

The use of neural networks for CPT-based liquefaction screening

Yusuf Erzin · Nurhan Ecemis

Received: 18 October 2013 / Accepted: 2 April 2014 / Published online: 24 April 2014

Abstract This study deals with development of two different artificial neural network (ANN) models: one for predicting cone penetration resistance and the other for predicting liquefaction resistance. For this purpose, cone penetration numerical simulations and cyclic triaxial tests conducted on Ottawa sand–silt mixes at different fines content were used. Results obtained from ANN models were compared with simulation and experimental results and found close to them. In addition, the performance indices such as coefficient of determination, root mean square error, mean absolute error, and variance were used to check the prediction capacity of the ANN models developed. Both ANN models have shown a high prediction performance based on the performance indices. It has been demonstrated that the ANN models developed in this study can be employed for predicting cone penetration and liquefaction resistances of sand–silt mixes quite efficiently.

Keywords Artificial neural networks · Cone penetration resistance · Liquefaction resistance · Ottowa sand

Introduction

An earthquake is a kind of natural disaster that occurs frequently around the world (Venkatesh et al. 2013). Liquefaction is one of the most destructive phenomena caused by earthquakes, and often occurs in loose, saturated soil deposits (Lee and Chern 2013). Liquefaction is defined as the transformation of a granular material from a solid to a liquefied state as a consequence of increased pore-water pressure and reduced effective stress (Marcuson 1978; Pathak and Dalvi 2011). Examples of liquefaction include the earthquakes in Niigata, 1964; Alaska, 1995; Loma Prieta, 1989; Kobe, 1995; Turkey, 1999; Chi–Chi, Twain, 1999; and Honshu, Japan, 2011. Liquefaction is observed to cause building settlement or tipping, landslides, dam instability, highway embankment failures, or other hazards (Pathak and Dalvi 2011). Such damages are generally of great concern to public safety and are of economic significance (Pathak and Dalvi 2011). In view of these serious damages caused by earthquake induced liquefaction, geotechnical engineers are actively engaged in the study of the soil liquefaction caused by earthquakes (Lee and Chern 2013). Thus, the assessment of the liquefaction potential due to an earthquake at a site is the first necessary step in liquefaction studies (Pathak and Dalvi 2011).

Geotechnical engineers have developed many assessment methods for evaluating soil liquefaction (Chern et al. 2008). Many of existing assessment methods was developed from the observations of the behavior of sites during earthquakes. Geotechnical engineers have often used the simple liquefaction analytical model developed by standard penetration test (SPT), due to its computational speed and analytical ability. Based on recent developments in data processing and analytical ability, the cone penetration test (CPT) offers the advantages of fast, continuous, and accurate soil parameter measurements. At the same time, the related testing data continued to accumulate. Thus, the potential of applying CPT to liquefaction research has grown significantly.

Y. Erzin (✉)
Department of Civil Engineering, Faculty of Engineering, Celal Bayar University, 45140 Manisa, Turkey
e-mail: yusuf.erzin@gmail.com

N. Ecemis
Department of Civil Engineering, Faculty of Engineering, Izmir Institute of Technology, 35430 Izmir, Turkey

A number of CPT-based liquefaction triggering resistance curves have been suggested by previous studies (e.g., Robertson and Campanella 1985; Seed and De Alba 1986; Shibata and Teparaska 1988; Andrus and Youd 1989; Stark and Olson 1995; Robertson and Wride 1998; Juang et al. 2003; Idriss and Boulanger 2004; Kokusho et al. 2005). The final accepted liquefaction screening method based on CPT has been developed by Robertson and Wride (1998). This method have been documented in the form of normalized cone penetration resistance (q_{c1N}) versus cyclic resistance ratio (CRR) induced by the earthquakes, corrected for 7.5 magnitude ($M_w = 7.5$), for many sites where liquefaction problem has been observed or not observed during the earthquakes (Fig. 1). Liquefaction resistance determined in this way depends only to the fines content (FC) of the soil for a known q_{c1N}. The clean sand boundary curve is adjusted for fines based on soil behavior type index, I_c. Figure 1 shows the resulting equivalent CRR curves for I_c values of 1.64, 2.07 and 2.59 which represent approximate apparent FC of 5, 15 and 35 %, respectively. Lately, it has been observed that a unique correlation between liquefaction resistance and penetration resistance is not possible to justify without considering the effects of hydraulic conductivity, k, compressibility, m_v, and coefficient of consolidation, c_h on penetration resistance (Thevanayagam and Ecemis 2008). The combined effect of the rate of penetration, v, geometry of the cone, d, and coefficient of consolidation, c_h also influence cone penetration resistance. Recently studied CPT numerical simulations (Thevanayagam and Ecemis 2008) and cyclic triaxial test results on Ottawa sand–silt mix (Thevanayagam et al. 2003) explored a unique correlation between liquefaction resistance and penetration resistance by considering the effects of the non-dimensional parameter $T(=vd/c_h)$ on cone penetration resistance.

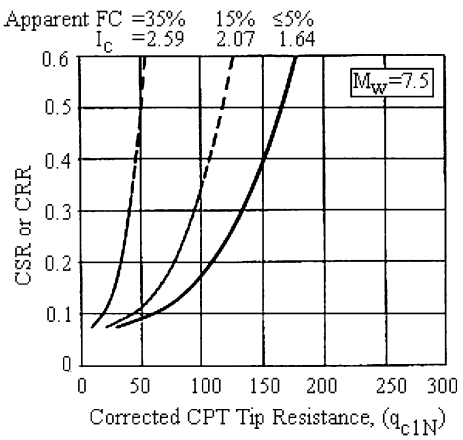

Fig. 1 Field liquefaction screening chart—CPT (Robertson and Wride 1998)

Artificial Neural Networks (ANNs) offer an interesting approach for modeling soil behavior (Shahin et al. 2001). ANN is an oversimplified simulation of the human brain (Banimahd et al. 2005) and is accepted as a reliable data-modelling tool to capture and represent complex relationships between inputs and outputs (Caglar and Arman 2007). This is in contrast to most traditional empirical and statistical methods, which need prior knowledge about the nature of relationships among the data (Shahin et al. 2008). Thus, ANNs are well suited to modeling the complex behavior of most geotechnical engineering materials which, by their very nature, exhibit extreme variability (Shahin et al. 2008). This modeling capability, as well as the ability to learn from experience, have given ANNs superiority over most traditional methods since there is no need for making assumptions about what the underlying rules that govern the problem in hand could be (Shahain et al. 2008). Since the early 1990s, ANNs have been effectively applied to almost every problem in geotechnical engineering (Shahain et al. 2008), including constitutive modeling (Najjar and Ali 1999; Penumadu and Zhao 1999); geo-material properties (Ozer et al. 2008; Erzin et al. 2009; Park and Kim 2010); bearing capacity of pile (Das and Basudhar 2006; Park and Cho 2010); slope stability (Zhao 2008; Cho 2009; Erzin and Cetin 2012, 2013, 2014), shallow foundations (Shahin et al. 2005; Erzin and Gul 2012, 2013), and tunnels and underground openings (Shi 2000; Yoo and Kim 2007). The ANN approach was also found to be suitable in the field of liquefaction potential assessment by various researchers such as Goh (1994, 1996, 2002), Juang and Chen (1999), Juang et al. (1999), Wang and Rahman (1999), Barai and Agarwal (2002), Baziar and Nilipour (2003), Neaupane and Achet (2004), Baziar and Ghorbani (2005), Das and Basudhar (2006), Young-Su and Byung-Tak (2006), Hanna et al. (2007a, b), Rao and Satyam (2007), Ramakrishnan et al. (2008), Farrokhzad et al. (2010), Pathak and Dalvi (2011), Moradi et al. (2011), Kumar et al. (2012), Venkatesh et al. (2013).

In this study, ANNs, with respect to the above advantages, were utilized both to investigate the influence of soil properties, namely, equivalent relative density $[(D_{rc})_{eq}]$, hydraulic conductivity (k) and compressibility (m_v) on normalized cone penetration resistance (q_{c1N}) and to investigate the unique correlation between cyclic resistance ratio (CRR) and q_{c1N} by considering the effects of non-dimensional parameter $T(=vd/c_h)$ on cone penetration resistance. For this purpose, two different ANN models were developed: one for the prediction of q_{c1N} (designated as ANN-1) and the other for the prediction of CRR (ANN-2). To achieve this, the results of CPT numerical simulations conducted using finite element code ABAQUS (2000) were used in the ANN-1 model while undrained cyclic

triaxial tests on Ottawa sand–silt mixes were used in the ANN-2 model. The results obtained from ANN-1 and ANN-2 models were compared with the results from numerical simulations and experimental investigations, respectively, and found to be close to them. Moreover, the determination coefficient (R^2), the values of variance account for (VAF), the mean absolute error (MAE) and root mean square error (RMSE) indices were calculated to check the prediction performance of the ANN-1 and ANN-2 models developed. Both ANN models have shown high prediction performance according to the performance indices.

Artificial neural networks

Artificial neural networks (ANNs) are computational models, which are based on the information processing system of the human brain (Banimahd et al. 2005). The current interest in ANNs is largely due to their ability to mimic natural intelligence in its learning from experience (Zurada 1992; Fausett 1994). Many authors have described the structure and operation of ANNs (e.g., Hecht-Nielsen 1990; Maren et al. 1990; Zurada 1992; Fausett 1994; Ripley 1996). ANNs architectures are formed by three or more layers, which consist of an input layer, one or more hidden layers, and an output layer. Each layer consists of a number of interconnected processing elements (PEs), commonly referred to as neurons. The neurons interact with each other via weighted connections. Each neuron is connected to all the neurons in the next layer. In the input layer, data are presented to the network. The output layer holds the response of the network to the input. The hidden layers enable these networks to represent and compute complicated associations between inputs and outputs. This ANN architecture is commonly referred to as a fully interconnected feed-forward multi-layer perceptron (MLP). In addition, there is also a bias, which is only connected to the neurons in the hidden and output layers, with modifiable weighted corrections.

The number of hidden layers used depends on the degree of the complexity of the problem. ANNs with one or two hidden layers and adequate number of hidden neurons are found to be quite useful for most problems (Orbanić and Fajdiga 2003; Goh 1994; Sonmez et al. 2005). The number of neurons in the hidden layers depends on the nature of the problem. There are various methods to determine the number of neurons in the hidden layer (Hecht-Nielsen 1987; Hush 1989; Kaastra and Boyd 1996; Kanellopoulas and Wilkinson 1997; Grima and Babuska 1999; Haque and Sudhakar 2002). However, these methods present general guidelines only for selection of an adequate number of neurons.

The neural network "learns" by modifying the weights of the neurons in response to the errors between the actual output values and the target output values. Several learning algorithms have been developed. The back-propagation learning algorithm is the most commonly used neural network algorithm (Rumelhart et al. 1986; Goh 1994; Najjar et al. 1996; Kim et al. 2004; Singh et al. 2006; Erzin et al. 2008). The back-propagation neural network has been applied with great success to model many phenomena in the field of geotechnical engineering (Goh 1995a, b; Shahin et al. 2002, 2001). In the back-propagation neural network, learning is carried out through gradient descent on the sum of the squares of the errors for all the training patterns (Rumelhart et al. 1986; Goh 1995a). Each neuron in a layer receives and processes weighted inputs from neurons in the previous layer and transmits its output to neurons in the following layer through links. Each link is assigned a weight which is a numerical estimate of the connection strength. The weighted summation of inputs to a neuron is converted to an output according to a nonlinear transfer function. The common transfer function widely used in the literature is the sigmoid function. The changes in the weights are proportional to the negative of the derivative of the error term. One pass through the set of training patterns, together with the associated updating of the weights, is called a cycle or an epoch. Training is carried out by repeatedly presenting the entire set of training patterns (updating the weights at the end of the each epoch) until the average sum squared error over all the training patterns is minimal and within the tolerance specified for the problem.

At the end of the training phase, the neural network should correctly reproduce the target output values for the training data; provided errors are minimal (i.e., convergence occurs). The associated trained weights of the neurons are then stored in the neural network memory. In the next phase, the trained neural network is fed a separate set of data. In this testing phase, the neural network predictions using the trained weights are compared to the target output values. The performance of the overall ANN model can be assessed by several criteria (Shi 2000; Shahin et al. 2004; Banimahd et al. 2005; Shahin and Jaksa 2005). These criteria include coefficient of determination R^2, mean squared error, mean absolute error, minimal absolute error, and maximum absolute error. A well-trained model should result in an R^2 close to 1 and small values of error terms.

In this study, determination of cone penetration and liquefaction resistances has been modeled using the ANN in which network training was accomplished with the neural network toolbox written in the Matlab environment (Math Works 7.0 Inc. 2006) and the Levenberg–Marquardt back-propagation learning algorithm (Demuth et al. 2006) was used in the training stage. Details of the experimental

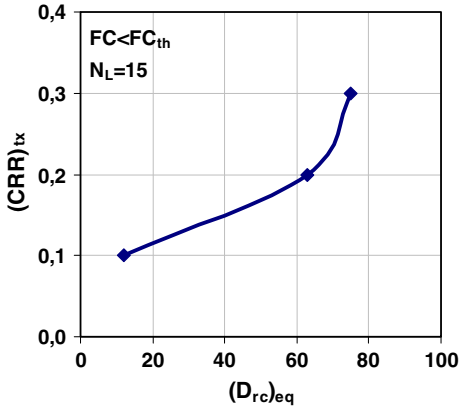

Fig. 2 $(CRR)_{tx} - (D_{rc})_{eq}$ for $N_L = 15$

investigations and numerical simulations, which have yielded the data for these models, are presented in the following sections.

Experimental investigations

An extensive experimental research was completed at State University of New York at Buffalo on cyclic resistance of sands and silty sands prepared at different silt contents (Thevanayagam et al. 2003). It involved several undrained cyclic triaxial tests on Ottawa sand (OS#55), non-plastic silt (Sil co sil #40) and their mixes at silt content (FC) of 0, 15 and 25 % by dry weight named OS-00, OS-15 and OS-25, respectively (Kanagalingam 2006). The number of equal stress cycles (N_L) required to reach ±5 % strain level (ε) at predefined CRR($=\Delta\sigma_v'/2\sigma_c'$) of 0.1, 0.2 or 0.3 and 100 kPa initial effective confining stress (σ_{vo}') was determined for each test. Where $\Delta\sigma_v'$ is deviator stress and σ_c' is the effective confining stress. Based on these undrained cyclic triaxial test data for Ottawa sand–silt mixes, a relationship between the undrained laboratory liquefaction resistance $(CRR)_{tx}$ required to cause liquefaction in 15 cycles ($N_L = 15$) and $(D_{rc})_{eq}$ has been developed for silty sands at FC less than threshold silt content (FC_{th}), as shown in Fig. 2 (Thevanayagam and Ecemis 2008). By using Fig. 2, $(CRR)_{tx}$ values were determined for equivalent relative density $(D_{rc})_{eq}$ values of the samples used in cyclic triaxial tests and presented in Table 1. In this table, column 5 lists the $(D_{rc})_{eq}$ values. $(D_{rc})_{eq}$ has been defined as (Thevanayagam 2007a, b);

$$(D_{rc})_{eq} = \frac{e_{max} - (e_c)_{eq}}{e_{max} - e_{min}}, \quad (1)$$

where e_{max} and e_{min} are maximum and minimum void ratio of the coarse grains, respectively. $(e_c)_{eq}$ is the equivalent void ratio and used for soils at FC less than FC_{th} $(e_c)_{eq}$ has been defined (Thevanayagam 2007a, b) in Eq. 2. In Eq. 2, f_c is the fines content by weight and b is the constant depending on grain size characteristics of the soil.

$$(e_c)_{eq} = \frac{e + (1-b)f_c}{1 - (1-b)f_c} \quad (2)$$

The field liquefaction resistance $(CRR)_{field}$ may be different from $(CSR)_{tx}$ depending on consolidation characteristics and the soil profile at a site. Furthermore, multi-directional shaking and modes of shear also differ from the laboratory. The latter aspects have been studied and corrections (Eq. 3) have been proposed by Castro (1975) and Seed et al. (1978). In Eq. 3, $K_o(=1 - \sin\phi)$ is the coefficient of lateral earth pressure at rest, ϕ is the soil friction angle. $(CRR)_{field}$ values were calculated by using Eq. 3 and given in Table 1, Column 10.

$$(CRR)_{field} = 0.9\frac{2(1+2K_o)}{3\sqrt{3}}(CRR)_{tx} \quad (3)$$

Numerical simulations

In order to study the effect of k, m_v and $(D_{rc})_{eq}$ on cone penetration resistance of sand and silty soils, several sets of numerical simulations were conducted using finite element code ABAQUS (2000) (Ecemis 2008). In each case, material properties required for the Drucker–Prager model were obtained from several sets of monotonic triaxial test data on Ottawa sand and sand–silt mixes prepared by mixing Ottawa sand with silt (Kanagalingam 2006; Thevanayagam et al. 2003). Cone penetration resistances were monitored with penetration of the cone diameter of 4.37 cm at a constant penetration speed of $v = 2$ cm/s (ASTM D3441) until a steady state condition was reached. The q_{c1N} at the tip of the cone was recorded against a non-dimensional parameter $T(=vd/c_h)$ with a range of c_h for a single soil type at different $(D_{rc})_{eq}$. The summary of the numerical simulation results are presented in Table 2.

Development of ANN model for prediction of cone penetration resistance

As mentioned earlier, the soil properties such as equivalent relative density $(D_{rc})_{eq}$, hydraulic conductivity (k), and compressibility (m_v) of silty sands affect normalized cone penetration resistance (q_{c1N}). Keeping this in view, an ANN model (designated as ANN-1) with three input parameters [$(D_{rc})_{eq}$, k, and m_v] and one output parameter (q_{c1N}) was developed for predicting q_{c1N}. The details of the input and output parameters of the ANN-1 model are listed in Table 3. The input and output data were scaled to lie between 0 and 1, by using Eq. 4.

Table 1 Summary of CRR—cyclic triaxial test results for Ottawa sand–silt mixes (Kanagalingam 2006)

(1) Sample no.	(2) FC (%)	(3) e_{max}	(4) e_{min}	(5) $(e_c)_{eq}$	(6) $(D_{rc})_{eq}$	(7) ϕ (°)	(8) K_o	(9) $(CRR)_{tx}$	(10) $(CRR)_{field}$
OS-00	0	0.8	0.6	0.675	63	32	0.47	0.226	0.152
				0.684	58	32	0.47	0.200	0.134
				0.604	98	36	0.41	1.582	1.000
				0.646	77	36	0.41	0.475	0.300
				0.675	63	32	0.47	0.226	0.152
				0.684	58	32	0.47	0.200	0.134
				0.604	98	36	0.41	1.582	1.000
				0.646	77	36	0.41	0.475	0.300
				0.675	63	32	0.47	0.226	0.152
				0.684	58	32	0.47	0.200	0.134
				0.604	98	36	0.41	1.582	1.000
				0.646	77	36	0.41	0.475	0.300
				0.675	63	32	0.47	0.226	0.152
				0.684	58	32	0.47	0.200	0.134
				0.604	98	36	0.41	1.582	1.000
				0.646	77	36	0.41	0.475	0.300
				0.675	63	32	0.47	0.226	0.152
				0.684	58	32	0.47	0.200	0.134
				0.604	98	36	0.41	1.582	1.000
				0.646	77	36	0.41	0.475	0.300
				0.675	63	32	0.47	0.226	0.152
				0.684	58	32	0.47	0.200	0.134
				0.604	98	36	0.41	1.582	1.000
				0.646	77	36	0.41	0.475	0.300
				0.675	63	32	0.47	0.226	0.152
				0.684	58	32	0.47	0.200	0.134
OS-15	15	0.75	0.43	0.780	10	29	0.52	0.100	0.070
				0.710	45	31	0.48	0.172	0.117
				0.780	10	29	0.52	0.100	0.070
				0.780	10	29	0.52	0.100	0.070
				0.710	45	31	0.48	0.172	0.117
				0.780	10	29	0.52	0.100	0.070
				0.780	10	29	0.52	0.100	0.070
				0.710	45	31	0.48	0.172	0.117
				0.780	10	29	0.52	0.100	0.070
				0.710	45	31	0.48	0.172	0.117
				0.780	10	29	0.52	0.100	0.070
OS-25	25	0.86	0.31	0.730	38	34	0.44	0.150	0.098
				0.730	38	34	0.44	0.150	0.098
				0.730	38	34	0.44	0.150	0.098
				0.730	38	34	0.44	0.150	0.098
				0.730	38	34	0.44	0.150	0.098

$$x_{norm} = \frac{(x - x_{min})}{(x_{max} - x_{min})}, \tag{4}$$

where x_{norm} is the normalized value, x is the actual value, x_{max} is the maximum value and x_{min} is the minimum value.

The data was then divided into two subsets; a training set, to construct the neural network model, and an independent validation set to estimate model performance in the deployed environment. Therefore, in total, 80 % of the

Table 2 Summary of CPT numerical simulation results (Ecemis 2008)

(1) Sample no.	(2) FC (%)	(3) $(D_{rc})_{eq}$ (%)	(4) m_v (kPa^{-1})	(5) k (m/sec)	(6) c_h (m^2/sec)	(7) T (vd/c_h)	(8) q_{c1N}
OS-00	0	98	0.000026	1.E−03	3.85718	0.000227	234.34
				1.E−04	0.38572	0.002266	225.24
				1.E−05	0.03857	0.022659	203.29
				1.E−07	0.00039	2.265907	83.62
				1.E−08	0.00004	22.65907	90.94
		77	0.000047	1.E−03	2.15200	0.000406	163.49
				1.E−04	0.21520	0.004061	164.01
				1.E−05	0.02152	0.040613	143.19
				1.E−06	0.00215	0.406134	70.77
				1.E−07	0.00022	4.06134	39.74
				1.E−08	0.00002	40.6134	53.48
		63	0.000033	1.E−02	31.27534	2.79E−05	110.24
				1.E−03	3.12753	0.000279	110.31
				1.E−04	0.31275	0.002795	111.01
				1.E−05	0.03128	0.027945	97.72
				1.E−06	0.00313	0.279453	51.27
				1.E−07	0.00031	2.794534	42.51
				1.E−08	0.00003	27.94534	45.69
		58	0.000035	1.E−02	28.85831	3.03E−05	117.25
				1.E−03	2.88583	0.000303	116.91
				1.E−04	0.28858	0.003029	109.29
				1.E−05	0.02886	0.030286	89.55
				1.E−06	0.00289	0.302859	44.22
				1.E−07	0.00029	3.028591	48.17
				1.E−08	0.00003	30.28591	52.00
OS-15	15	45	0.000035	1.E−03	2.89155	0.000302	25.69
				1.E−05	0.02892	0.030226	25.15
				1.E−07	0.00029	3.0226	23.58
				1.E−08	0.00003	30.226	23.14
		10	0.000062	1.E−02	16.48375	5.3E−05	7.07
				1.E−03	1.64837	0.00053	7.16
				1.E−04	0.16484	0.005302	17.33
				1.E−05	0.01648	0.053022	15.57
				1.E−06	0.00165	0.530219	14.46
				1.E−07	0.00016	5.302193	11.06
				1.E−08	0.00002	53.02193	10.39
OS-25	25	38	0.000096	1.E−03	1.06416	0.000821	7.48
				1.E−05	0.01064	0.08213	7.71
				1.E−06	0.00106	0.821302	7.95
				1.E−07	0.00011	8.213023	6.94
				1.E−08	0.00001	82.13023	7.29

data were used for training and 20 % for testing. It has been shown that a network with one hidden layer can approximate any continuous function, provided that sufficient connection weights are used (Hornik et al. 1989). Consequently, one hidden layer was used. The neural network toolbox of MATLAB7.0, a popular numerical computation and visualization software (Banimahd et al. 2005), was used for training and testing of MLPs. The optimum number of neurons in the hidden layer was determined by varying their number by starting with a minimum of 1 and then increasing the network size in steps by adding 1 neuron each time. Different transfer functions (such as log-sigmoid (Sakellariou and Ferentinou 2005) and tan-sigmoid (Orbanić and Fajdiga 2003) were

investigated to achieve the best performance in training as well as in testing. Two momentum factors, μ (=0.01 and 0.001) were selected for the training process to search for the most efficient ANN architecture. Training started with a small number of epochs (=50) and kept on incrementing by 50 epochs until the onset of specialized training as reflected in the reversal of the downward trend of the error for testing data. The maximum number of epochs to train was chosen as 500. The coefficient of determination, R^2, and the mean absolute error, MAE, were used to evaluate the performance of the developed ANN models. In order to determine the optimum network geometry, the performance of the network during the training and testing processes was examined for each network size until no significant improvement occurred.

Table 3 The details of the parameters used for the ANN-1 model developed

Parameters used	Minimum	Maximum	Mean	SD
Input parameters				
$(D_{rc})_{eq}$ (%)	10	98	54.6098	26.7739
k (m/sec)	1E−08	0.01	91.6E−05	26.11E−04
m_v (kPa^{-1})	2.6E−05	9.6E−05	4.74E−5	2.15E−5
Output parameter				
q_{c1N}	6.94	234.34	70.7562	63.3877

The details of the optimal performance of the networks are given in Table 4. Table 4 shows that ANN with six hidden neurons resulted in the maximum R^2 of 0.9883 and the minimum MAE of 6.38 in the testing phase. Therefore, it was chosen as the best ANN model. Connection weights and biases for the final model are presented in Table 5.

As mentioned earlier, the test data was randomly selected and the remaining part was accepted as the training data while developing the optimal ANN-1 model. In addition to this, this sampling phase was performed for four times ($n = 4$) by using different train/test samples. The iterations for prediction were performed for each different train/test samples and the results were presented in Table 6. It can be seen from the table that all the models from $n = 1$ to $n = 4$ exhibit good prediction performance. When comparing the prediction performances of these models with the optimal ANN-1 model, the optimal ANN-1 model yields the highest prediction performance.

Development of ANN model for prediction of liquefaction resistance

As mentioned earlier, there is a unique correlation between liquefaction resistance (CRR), normalized cone penetration resistance (q_{c1N}) and non-dimensional parameter (T). Keeping this in view, an ANN model (designated as ANN-2)

Table 4 Details of the optimal performance of networks in predicting q_{c1N}

Number of neurons in the hidden layer	Transfer function in		μ	Number of epochs	Training		Testing	
	Neurons of the hidden layer	Neurons of the output layer			R^2	MAE	R^2	MAE
1	Tan-sigmoid	Log-sigmoid	0.001	100	0.3025	49.89	0.5857	60.66
2	Tan-sigmoid	Tan-sigmoid	0.001	100	0.4211	46.85	0.5857	56.95
3	Tan-sigmoid	Tan-sigmoid	0.001	100	0.9865	4.85	0.7437	23.81
4	Tan-sigmoid	Tan-sigmoid	0.001	140	0.9822	4.48	0.7949	21.46
5	Tan-sigmoid	Tan-sigmoid	0.001	190	0.9846	3.86	0.8175	20.37
6	Tan-sigmoid	Tan-sigmoid	0.001	340	0.9960	2.18	0.9883	6.38

Table 5 Connection weights and biases of the best ANN model

Hidden neuron	Weights				Bias	
	Input neurons			Output neuron	Hidden layer	Output layer
	$(D_{rc})_{eq}$	k	m_v	q_{c1N}		
1	1.2023	1.0096	4.1967	13.4256	−3.6485	−10.4978
2	−2.6187	0.0277	−3.8974	−9.5281	−2.0850	
3	−0.7382	29.7529	−0.1046	−13.4605	29.8829	
4	−9.5339	−1.0874	0.7208	−1.9402	−7.2946	
5	−2.8259	7.7121	−3.2265	10.8344	6.0833	
6	0.3763	−52.1087	0.1524	−29.713	−53.0366	

Table 6 Details of the performance of networks for different train/test samples

Model	Number of neurons in the hidden layer	Transfer function in		μ	Number of epochs	Training		Testing	
		Neurons of the hidden layer	Neurons of the output layer			R^2	MAE	R^2	MAE
$n = 1$	6	Tan-sigmoid	Log-sigmoid	0.001	300	0.9827	8.09	0.9699	5.34
$n = 2$	6	Tan-sigmoid	Tan-sigmoid	0.001	500	0.9800	8.79	0.9471	11.25
$n = 3$	6	Tan-sigmoid	Tan-sigmoid	0.001	160	0.9771	8.99	0.9362	11.40
$n = 4$	6	Tan-sigmoid	Tan-sigmoid	0.001	250	0.9573	11.19	0.9526	11.36
Optimal ANN-1	6	Tan-sigmoid	Tan-sigmoid	0.001	340	0.9960	2.18	0.9883	6.38

Table 7 The details of the parameters used for the ANN-2 model developed

Parameters used	Minimum	Maximum	Mean	SD
Input parameters				
T	2.79E−5	82.013	7.5492	17.0915
q_{c1N}	6.94	234.34	70.7562	63.3877
Output parameter				
$(CRR)_{field}$	0.07	1.00	0.2679	0.3104

with two input parameters (T and q_{c1N}) and one output parameter [$(CRR)_{field}$] was developed for predicting $(CRR)_{field}$. The details of the input and output parameters of the ANN-2 model are listed in Table 7. The input and output data were scaled to lie between 0 and 1, by using Eq. 4.

The data was then divided into two subsets; a training set and independent validation set. Therefore, in total, 80 % of the data were used for training and 20 % for testing. One hidden layer was chosen. During the design of optimal ANNs, the trials were formed similar to the trials made in modeling of cone penetration resistance (see "Development of ANN model for prediction of cone penetration resistance" section). The details of the optimal performance of the networks are given in Table 8. Table 8 shows that ANN with five hidden neurons resulted in the maximum R^2 of 0.9983 and the minimum MAE of 0.01 in the testing phase. Connection weights and biases for the optimal ANN model are presented in Table 9.

As in the ANN-1 model, the test data was randomly selected and the remaining part was accepted as the training data while developing the optimal ANN-2 model. In addition to this, this sampling phase was performed for four times ($n = 4$) by using different train/test samples. The iterations for prediction were performed for each different train/test samples and the results are presented in Table 10. It can be seen from the table that all the models from $n = 1$ to $n = 4$ exhibit good prediction performance. When comparing the prediction performances of these models with the optimal ANN-2 model, the optimal ANN-2 model yields the highest prediction performance.

Results and discussion

A comparison of numerical results with the results obtained from the ANN-1 model developed for the prediction of q_{c1N} is depicted in Figs. 3 and 4 for training and testing samples, respectively. It can be noted from these figures that q_{c1N} values obtained from ANN model are in good agreement with the numerically obtained q_{c1N} values, as their R^2 is much closer to unity. This shows that the ANN model is able to predict cone penetration resistances of sand–silt mixes, if their physical properties [$(D_{rc})_{eq}$, k, and m_v] are known.

Table 8 Details of the optimal performance of networks in predicting $(CRR)_{field}$

Number of neurons in the hidden layer	Transfer function in		μ	Number of epochs	Training		Testing	
	Neurons of the hidden layer	Neurons of the output layer			R^2	MAE	R^2	MAE
1	Tan-sigmoid	Tan-sigmoid	0.001	100	0.5443	0.13	0.6360	0.13
2	Tan-sigmoid	Tan-sigmoid	0.001	200	0.9671	0.04	0.9616	0.06
3	Tan-sigmoid	Tan-sigmoid	0.001	100	0.9860	0.02	0.9791	0.03
4	Tan-sigmoid	Tan-sigmoid	0.001	380	0.9923	0.02	0.9936	0.02
5	Tan-sigmoid	Tan-sigmoid	0.001	240	0.9988	0.01	0.9983	0.01

Table 9 Connection weights and biases of the best ANN model

Hidden neuron	Weights			Bias	
	Input neurons		Output neuron	Hidden layer	Output layer
	T	q_{c1N}	$(CRR)_{field}$		
1	11.8511	−12.5340	−1.3987	−0.6636	0.8814
2	−0.9000	−4.9676	−9.6192	−1.6168	
3	102.8228	−4.0986	10.5454	102.3089	
4	−138.8900	−15.5882	−1.1691	−136.0383	
5	−0.8074	−9.8285	−3.3869	5.1425	

Table 10 Details of the performance of networks for different train/test samples

Model	Number of neurons in the hidden layer	Transfer function in		μ	Number of epochs	Training		Testing	
		Neurons of the hidden layer	Neurons of the output layer			R^2	MAE	R^2	MAE
$n = 1$	5	Tan-sigmoid	Log-sigmoid	0.001	200	0.9951	0.01	0.9822	0.03
$n = 2$	5	Tan-sigmoid	Tan-sigmoid	0.001	80	0.9930	0.05	0.9784	0.03
$n = 3$	5	Tan-sigmoid	Tan-sigmoid	0.001	78	0.9797	0.05	0.9731	0.03
$n = 4$	5	Tan-sigmoid	Tan-sigmoid	0.001	160	0.9959	0.05	0.9585	0.03
Optimal ANN-2	5	Tan-sigmoid	Tan-sigmoid	0.001	340	0.9988	0.01	0.9983	0.01

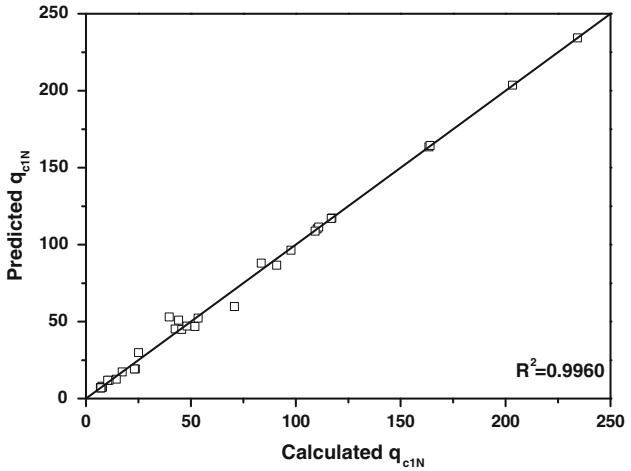

Fig. 3 Comparison of the q_{c1N} values calculated from numerical simulations with the q_{c1N} values predicted from the ANN-1 model for training samples

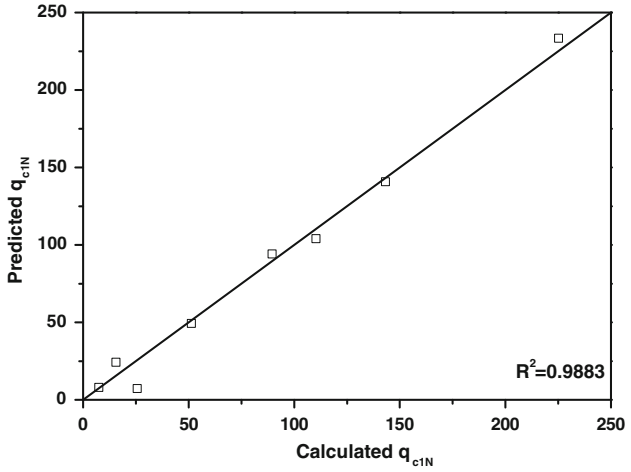

Fig. 4 Comparison of the q_{c1N} values calculated from numerical simulations with the q_{c1N} values predicted from the ANN-1 model for testing samples

Correlations were also calculated between input and output parameters used in the ANN-1 model to show the relation between the parameters. The correlation coefficients, r, values calculated are given in Table 11. Smith (1986) suggested the following guide for values of $|r|$ between 0.0 and 1.0:

$|r| \geq 0.8$ Strong correlation exists between the two sets of variables;

$0.2 < |r| < 0.8$ Correlation exists between the two sets of variables;

$|r| \leq 02$ Weak correlation exists between the two sets of variables.

The r values in Table 11 are smaller than 0.8, which indicate that there is not a strong correlation between the parameters causing them to achieve the performance results of the ANN-1 model. This result also indicates that

Table 11 Correlation coefficients of each input and the output one by one for ANN-1 model

Output parameter	Input parameters		
	$(D_{rc})_{eq}$	k	m_v
q_{c1N}	0.780	0.075	0.554

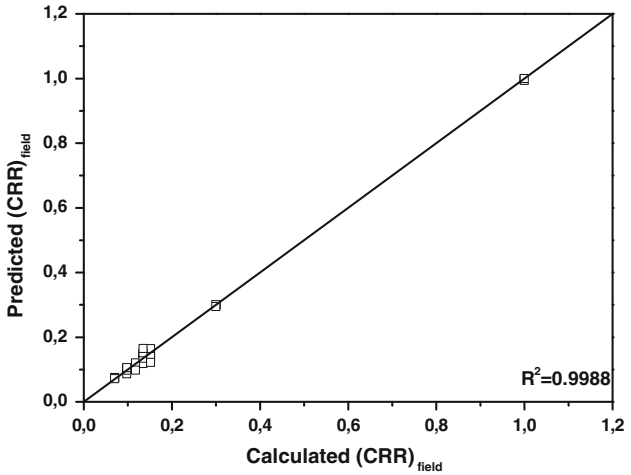

Fig. 5 Comparison of the $(CRR)_{field}$ values calculated from cyclic triaxial tests with the $(CRR)_{field}$ values predicted from ANN-2 model for training samples

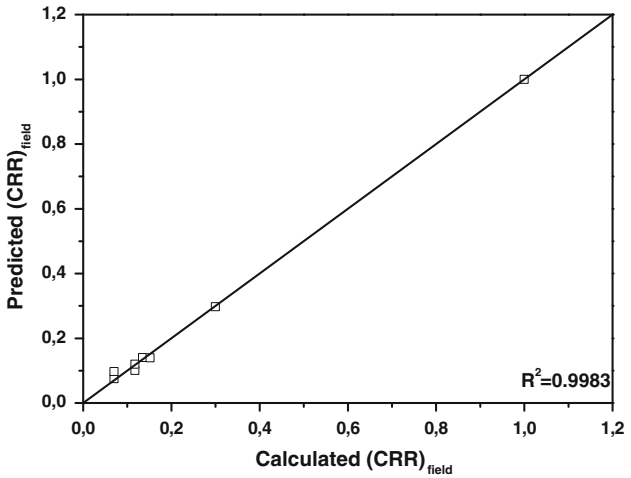

Fig. 6 Comparison of the $(CRR)_{field}$ values calculated from cyclic triaxial tests with the $(CRR)_{field}$ values predicted from the ANN-2 model for testing samples

ANN is a reliable data modeling tool to capture and represent complex relationships between input and output parameters.

A comparison of $(CRR)_{field}$ values calculated by using Eq. 3 with the results obtained from the ANN-2 model developed is depicted in Figs. 5 and 6 for training and testing samples, respectively. It can be noticed from these figures that $(CRR)_{field}$ values obtained from the ANN model are quite close to the calculated $(CRR)_{field}$ values, as their R^2 values are much closer to unity. This shows that the ANN model is able to predict liquefaction resistances of sand–silt mixes, if their T and q_{c1N} values are known. If q_{c1N} values are unknown, q_{c1N} values could be predicted by using trained ANNs values in this study. Correlations were also calculated between the input and output parameters used in the ANN-2 model to show the relation between the parameters. The correlation coefficient, r, values calculated are given in Table 12. The r values in Table 12 are smaller than 0.8, which indicate that there is not a strong correlation between the parameters causing them to achieve the performance results of the ANN-2 model. This result also indicates that ANN is a reliable data modeling tool to capture and represent complex relationships between input and output parameters as mentioned earlier.

$(CRR)_{field}$ values were then obtained from the Robertson and Wride (1998)'s liquefaction screening chart (Fig. 1) for the data used in this study and compared with the calculated $(CRR)_{field}$ values, as shown in Fig. 7. Figure 7 shows that $(CRR)_{field}$ values obtained from Fig. 1 are not in good agreement with calculated $(CRR)_{field}$ values for the data used in this study. This is possibly due to the fact that the $(CRR)_{field}$ determined from Fig. 1 depends only on the fines content of the soil, the determination of which is based on only CPT data. As pointed out by Finn (1993), Larsson et al. (1995) and Ziaie-Moayed et al. (2002), this determination of fines content of the silty sands might cause some uncertainty. Therefore, there will be probably some errors in evaluation of liquefaction resistances of sand–silt mixes using this method as pointed out by Ziaie-Moayed et al. (2002).

In fact, the coefficient of correlation between the measured and predicted values is a good indicator to check the prediction performance of the model (Gokceoglu and Zorlu 2004). In this study, variance VAF, represented by Eq. 5, and the root mean square error RMSE, represented by Eq. 6, were also computed to assess the performance of the developed models (Grima and Babuska 1999; Finol et al. 2001; Gokceoglu 2002; Erzin 2007; Erzin and Yukselen 2009; Erzin et al. 2008, 2009, 2010)

$$\mathrm{VAF} = \left[1 - \frac{\mathrm{var}(y - \hat{y})}{\mathrm{var}(y)}\right] \times 100, \tag{5}$$

$$\mathrm{RMSE} = \sqrt{\frac{1}{N}\sum_{i=1}^{N}(y_i - \hat{y}_i)^2}, \tag{6}$$

where var denotes the variance, y is the measured value, $\hat{y}$ is the predicted value, and N is the number of the sample. If VAF is 100 % and RMSE is 0, the model is treated as excellent.

Table 12 Correlation coefficients of each input and the output one by one for ANN-2 model

Output parameter	Input parameters	
	T	q_{c1N}
$(CRR)_{field}$	0.093	0.685

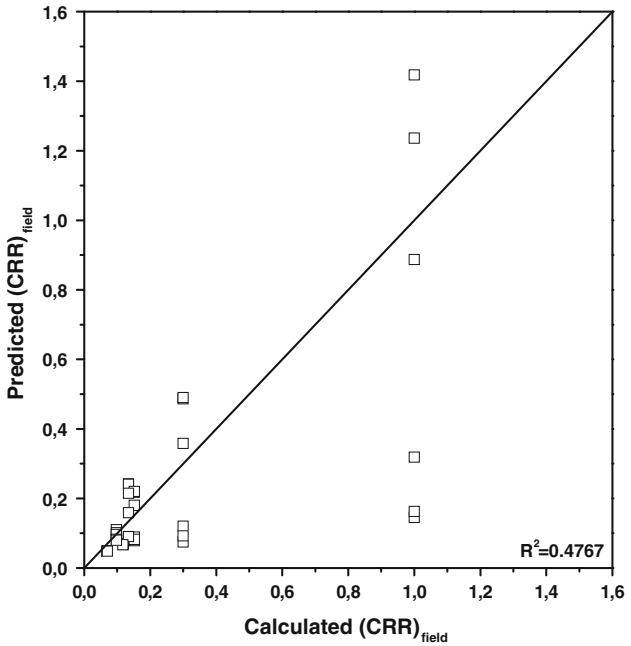

Fig. 7 Comparison of the $(CRR)_{field}$ values calculated from cyclic triaxial tests with the $(CRR)_{field}$ values predicted from the field liquefaction screening chart for all samples

Table 13 Performance indices (R^2, *RMSE*, *MAE* and *VAF*) of ANN-1 and ANN-2 models developed and the field liquefaction screening chart

Model	Data	R^2	RMSE	MAE	*VAF* (%)
ANN-1	Training set	0.9960	3.82	2.19	99.60
	Testing set	0.9883	8.29	6.38	98.62
ANN-2	Training set	0.9988	0.01	0.01	99.88
	Testing set	0.9983	0.01	0.01	99.83
The field liquefaction screening chart	All set	0.4767	0.24	0.13	41.66

Values of VAF and RMSE for the ANN-1 and ANN-2 models developed and Robertson and Wride (1998)'s liquefaction screening chart are listed in Table 13. It can be noted from Table 13 that both of the ANN models developed exhibit high prediction performance based on the performance indices, which demonstrates their usefulness and efficiency.

When comparing the performance of the ANN-2 model with the field liquefaction screening chart, the ANN-2 model is able to predict CRR much more efficiently. This is possibly due to the fact that the ANN-2 model takes into consideration the effect of non-dimensional parameter T including the combined effect of the parameters, namely, the rate of penetration (v), geometry of the cone (d), and coefficient of consolidation (c_h) influencing cone penetration resistance whereas, as mentioned earlier, the CRR determined from Fig. 1 depends only on the fines content of the soil, the determination of which is based on only CPT data, and might cause some uncertainty as observed by past researchers (Finn 1993; Larsson et al. 1995; and Ziaie-Moayed et al. 2002). These results also indicate that the ANN-2 model is able to predict liquefaction resistances quite efficiently and is superior to the liquefaction screening chart (Fig. 1) for the data used in this study.

As mentioned earlier in the "Experimental investigations" section, CRR can be also calculated by using Eq. (3). However, this determination of CRR is much more time consuming, expensive and involves destructive tests. Additionally, the determination of CRR by using the ANN-2 model is quick, cheap and involves nondestructive tests.

Neural Network applications are treated as black box applications in general (Cabalar and Cevik 2009; Cevik et al. 2011). Some researchers such as Cabalar and Cevik (2009), Cevik et al. (2011) and Köroğlu et al. (2013) opened this black box and introduced the NN application in a closed form solution by using related NN parameters such as weights and biases. Similarly, ANN-1 and ANN-2 models developed in this study can be expressed in explicit function form using the related NN parameters. Using the weights and biases of the optimal ANN-1 model (Table 5), normalized cone penetration resistance (q_{c1N}) can be expressed in terms of equivalent relative density $(D_{rc})_{eq}$, hydraulic conductivity (k), and compressibility (m_v) as follows:

$$q_{c1N} = (227.40 * \tanh\ W) + 6.94, \quad (7)$$

where $\tanh(x) = (e^x - e^{-x})/(e^x + e^{-x})$, and finally output is computed as:

$$\begin{aligned} W = {} & [13.4256 * \tanh U_1 - 9.5281 * \tanh U_2 \\ & - 13.4605 * \tanh U_3 - 1.9402 * \tanh U_4 \\ & + 10.8344 * \tanh U_5 - 29.7130 * \tanh U_6] - 10.4978 \\ U_1 = {} & 1.2023 * (D_{rc})_{eq} + 1.0096 * k + 4.1967 * m_v - 3.6485 \\ U_2 = {} & -2.6187 * (D_{rc})_{eq} + 0.0277 * k - 3.8974 * m_v - 2.0850 \\ U_3 = {} & -0.7382 * (D_{rc})_{eq} + 29.7529 * k - 0.1046 * m_v + 29.8829 \\ U_4 = {} & -9.5339 * (D_{rc})_{eq} - 1.0874 * k + 0.7208 * m_v - 7.2946 \\ U_5 = {} & -2.8259 * (D_{rc})_{eq} + 7.7121 * k - 3.2265 * m_v + 6.0833 \\ U_6 = {} & 0.3763 * (D_{rc})_{eq} - 52.1087 * k + 0.1524 * m_v - 53.0366 \end{aligned}$$

Similarly, using the weights and biases of the optimal ANN-2 model (Table 9), liquefaction resistance $(CRR)_{field}$ can be expressed in terms of the non-dimensional

parameter (T) and normalized cone penetration resistance (q_{c1N}) as follows:

$$(\mathrm{CRR})_{\mathrm{field}} = (0.93 * \tanh\ Y) + 0.07, \quad (8)$$

where

$$\begin{aligned} Y = {} & [-1.3987 * \tanh L_1 - 9.6192 * \tanh L_2 \\ & + 10.5454 * \tanh L_3 - 1.1691 * \tanh L_4 \\ & - 3.3869 * \tanh L_5] + 0.8814 \\ L_1 = {} & 11.8511 * T - 12.5340 * q_{c1N} - 0.6636 \\ L_2 = {} & -0.9000 * T - 4.9676 * q_{c1N} - 1.6168 \\ L_3 = {} & 102.8228 * T - 4.0986 * q_{c1N} + 102.3089 \\ L_4 = {} & -138.890 * T - 15.5882 * q_{c1N} - 136.0383 \\ L_5 = {} & -0.8074 * T - 9.8285 * q_{c1N} - 5.1425 \end{aligned}$$

It should be noted that the proposed ANN-1 and ANN-2 models in this study are valid for the ranges of parameters given in Tables 3 and 7, respectively. It should be also noted that the numerical simulations and the experimental investigations (Tables 1, 2), were taken from two PhD dissertations (Kanagalingam 2006 and Ecemis 2008) and so small data size were used while developing the ANN models, and it is not possible now to obtain the data for this problem at this stage.

Conclusions

In this study, two different ANN models have been developed: one for predicting cone penetration resistance (ANN-1) and the other for predicting liquefaction resistance (ANN-2). For this purpose, cyclic triaxial test results on Ottawa sand–silt mixes at different fines content have been used in the ANN-1 model, while CPT numerical simulation results have been used in the ANN-2 model. The ANN-1 model had three input parameters $(D_{rc})_{eq}$, k and m_v, and an output parameter, q_{c1N}. The ANN-2 model had two input parameters, T and q_{c1N} and an output parameter $(\mathrm{CRR})_{\mathrm{field}}$. The results of the ANN-1 model were compared with those obtained from experiments and found to be close to them. The results of the ANN-2 model were compared with those obtained from the numerical simulations and found to be good agreement with them. Further, $(\mathrm{CRR})_{\mathrm{field}}$ values obtained from the Robertson and Wride (1998)'s liquefaction screening chart for the data used in this study were compared with the calculated $(\mathrm{CRR})_{\mathrm{field}}$ values. It is found that the liquefaction screening chart based on fines content yielded poor predictions. In addition, the performance indices such as coefficient of determination, root mean square error, mean absolute error, and variance were used to assess the performance of the ANN-1 and ANN-2 models and the liquefaction screening chart. The study demonstrates that the ANN-1 and ANN-2 models are able to predict cone penetration and liquefaction resistances, respectively, quite efficiently, and the ANN-2 model is superior to the liquefaction screening chart since it depends only to the fines content of the soil.

References

Abaqus Inc (2000) Abaqus 6.1, user's manual. Hibbitt, Karlsson and Sorensen, Inc, Fremont, CA

Andrus RD, Youd TL (1989) Penetration test in liquefiable gravels. In: Proceedings of the 12th international conference on soil mechanics and foundation engineering, Rotterdam, the Netherlands, pp 679–682

ASTM (1993) Designation D3441—standard test method for deep quasi-static, cone, and friction cone penetration tests of soil. In: Annual book of ASTM standards soil and rock: building stones, vol 4.08, American Society for Testing and Materials, Philedalphia, PA

Banimahd M, Yasrobi SS, Woodward PK (2005) Artificial neural network for stress-strain behavior of sandy soils: Knowledge based verification. Comput Geotech 32:377–386

Barai S, Agarwal G (2002) Studies on instance based learning models for liquefaction potential assessment. EJGE. www.ejge.com/2002/Ppr0235/Ppr0235.htm

Baziar MH, Ghorbani A (2005) Evaluation of lateral spreading using artificial neural networks. Soil Dyn Earthq Eng 25:1–9

Baziar MH, Nilipour N (2003) Evaluation of liquefaction potential using neural-networks and CPT results. Soil Dyn Earthq Eng 23:631–636

Cabalar AF, Cevik A (2009) Modeling damping ratio and shear modulus of sand–mica mixtures using neural networks. Eng Geol 104:31–40

Caglar N, Arman H (2007) The applicability of neural networks in the determination of soil profiles. Bull Eng Geol Environ 66(3):295–301

Castro G (1975) Liquefaction and cyclic mobility of saturated sands. J Geotech Eng Div 101(6):551–569

Cevik A, Sezer EA, Cabalar AF, Gokceoglu C (2011) Modeling of the uniaxial compressive strength of some clay-bearing rocks using neural network. Appl Soft Comput 11(2):2587–2594

Chern S, Lee C, Wang C (2008) CPT-based liquefaction assessment by using fuzzy neural networks. J Mar Sci Tech 16(2):139–148

Cho SE (2009) Probabilistic stability analyses of slopes using the ANN-based response surface. Comput Geotech 36:787–797

Das SK, Basudhar PK (2006) Undrained lateral load capacity of piles in clay using artificial neural network. Comput Geotech 33(8):454–459

Demuth H, Beale M, Hagan M (2006) Neural network toolbox user's guide. The Math Works, Natick

Ecemis N (2008) Effects of permeability and compressibility on liquefaction screening using cone penetration resistance. Ph.D. dissertation, Department of Civil Structural and Environmental Engineering, State University of New York at Buffalo (SUNY)

Erzin Y (2007) Artificial neural networks approach for swell pressure versus soil suction behavior. Can Geotech J 44(10):1215–1223

Erzin Y, Cetin T (2012) The use of neural networks for the prediction of the critical factor of safety of an artificial slope subjected to earthquake forces. Sci Iran 19(2):188–194

Erzin Y, Cetin T (2013) The prediction of the critical factor of safety of homogeneous finite slopes using neural networks and multiple regressions. Computat Geosci 51:305–313

Erzin Y, Cetin T (2014) The Prediction of the critical factor of safety of homogeneous finite slopes subjected to earthquake forces using neural networks and multiple regressions. Int J Geomech Eng 6(1):1–15
Erzin Y, Gul T (2012) The use of neural networks for the prediction of the settlement of one-way footings on cohesionless soils based on standard penetration test. Neural Comput Appl. doi:10.1007/s00521-012-1302-x
Erzin Y, Gul T (2013) The use of neural networks for the prediction of the settlement of pad footings on cohesionless soils based on standard penetration test. Int J Geomech Eng 5(6):541–564
Erzin Y, Yukselen Y (2009) The use of neural networks for the prediction of zeta potential of kaolinite. Math Geosci 41:779–797
Erzin Y, Rao BH, Singh DN (2008) Artificial neural networks for predicting soil thermal Resistivity. Int J Therm Sci 47:1347–1358
Erzin Y, Gumaste SD, Gupta AK, Singh DN (2009) ANN models for determining hydraulic conductivity of compacted fine grained soils. Can Geotech J 46:955–968
Erzin Y, Rao BH, Patel A, Gumaste SD, Gupta AK, Singh DN (2010) Artificial neural network models for predicting of electrical resistivity of soils from their thermal resistivity. Int J Therm Sci 49:118–130
Farrokhzad F, Choobbasti AJ, Barari A (2010) Artificial neural network model for prediction of liquefaction potential in soil deposits. In: 5th International conference on recent advances in geotechnical earthquake engineering and soil dynamics and symposium in Honor of Prof. I. M. Idriss, paper no. 4.46a, pp 1–8
Fausett LV (1994) Fundamentals of neural networks: architecture, algorithms, and applications. Prentice-Hall, Englewood Cliffs
Finn WDL (1993) Evaluation of liquefaction potential. In: Proceedings of the conference on soil dynamics and geotechnical earthquake engineering, Balkema, Rotterdam
Finol J, Guo YK, Jing XD (2001) A rule based fuzzy model for the prediction of petrophysical rock parameters. J Petrol Sci Eng 29:97–113
Goh ATC (1994) Seismic liquefaction potential assessed by neural networks. J Geotech Geoenviron 120(9):1467–1480
Goh ATC (1995a) Back-propagation neural networks for modelling complex systems. Artif Intell Eng 9:143–151
Goh ATC (1995b) Modelling soil correlations using neural networks. J Comput Civil Eng 9:275–278
Goh ATC (1996) Neural network modelling of CPT seismic liquefaction data. J Geotech Eng 122(1):70–73
Goh ATC (2002) Probabilistic neural network for evaluating seismic liquefaction potential. Can Geotech J 39:219–223
Gokceoglu C (2002) A fuzzy triangular chart to predict the uniaxial compressive strength of Ankara agglomerates from their petrographic composition. Eng Geol 66(1–2):39–51
Gokceoglu C, Zorlu K (2004) A fuzzy model to predict the uniaxial compressive strength and the modulus of elasticity of a problematic rock. Eng Appl Artif Intel 17(1):61–72
Grima MA, Babuska R (1999) Fuzzy model for the prediction of unconfined compressive strength of rock samples. Int J Rock Mech Min 36:339–349
Hanna AM, Ural D, Saygili G (2007a) Neural network model for liquefaction potential in soil deposits using Turkey andTaiwan earthquake data. Soil Dyn Earthq Eng 27(6):521–540
Hanna AM, Ural D, Saygili G (2007b) Evaluation of liquefaction potential of soil deposits using artificial neural networks. Eng Comput 24(1):5–16
Haque ME, Sudhakar KV (2002) ANN back-propagation prediction model for fracture toughness in microalloy steel. Int J Fatigue 24:1003–1010
Hecht-Nielsen R (1987) Kolomogorov's mapping neural network existence theorem. In: Proceedings of the first IEEE international conference on neural networks, San Diego CA, USA, pp 11–14
Hecht-Nielsen R (1990) Neurocomputing. Addison-Wesley, Boston
Hornik K, Stinchcombe M, White H (1989) Multilayer feedforward networks are universal approximators. Neural Netw 2:359–366
Hush DR (1989) Classification with neural networks: a performance analysis. In: Proceedings of the IEEE international conference on systems engineering Dayton Ohia, USA, pp 277–280
Idriss IM, Boulanger RW (2004) Semi-empirical procedures for evaluating liquefaction potential during earthquakes. In: Proceedings of the 11th International Conference on Soil Dynamics and Earthquake Engineering and 3rd International Conference on Earthquake Geotechnical Engineering, Berkeley, California, pp 32–56
Juang CH, Chen CJ (1999) CPT-base liquefaction evaluation using artificial neural networks. Comput Aided Civ Inf 14:221–229
Juang CH, Chen CJ, Tien YM (1999) Appraising cone penetration test based liquefaction resistance evaluation methods: artificial neural network approach. Can Geotech J 36:443–454
Juang CH, Yuan H, Lee DH, Lin PS (2003) Simplified cone penetration test-based method for evaluating liquefaction resistance of soils. J Geotech Geoenviron Eng 129(1):66–80
Kaastra I, Boyd M (1996) Designing a neural network for forecasting financial and economic time series. Neurocomputing 10(3):215–236
Kanagalingam T (2006) Liquefaction resistance of granular mixes based on contact density and energy considerations. Ph.D. dissertation, State University of New York at Buffalo, Buffalo, NY
Kanellopoulas I, Wilkinson GG (1997) Strategies and best practice for neural network image classification. Int J Remote Sens 18:711–725
Kim H, Rauch AF, Haas CT (2004) Automated quality assessment of stone aggregates based on laser imaging and a neural network. J Comput Civil Eng 18(1):58–64
Kokusho T, Hara T, Murahata K (2005) Liquefaction strength of fines containing sands compared with cone resistance in triaxial specimens. In: Pre-workshop proceedings of the 2nd Japan–US workshop on testing, modelling, and simulation in geomechanics, Campus Plaza, Kyoto, Japan, pp 280–296
Köroğlu MA, Köken A, Arslan MH, Çevik A (2013) Neural network prediction of the ultimate capacity of shear stud connectors on composite beams with profiled steel sheeting. Sci Iran 20(4):1101–1113
Kumar V, Venkatesh K, Tiwari RP, Kumar Y (2012) Application of ANN to predict liquefaction potential. Int J Comput Eng Sci 2(2):379–389
Larsson R, Lofroth B, Moller B (1995) Processing of Data From CPT Tests. In: International symposium on cone penetration testing, CPT'95, Linkoping, Sweden, vol 2, pp 201–207
Lee C, Chern S (2013) Application of a support vector machine for liquefaction assessment. J Mar Sci Tech 21(3):318–324
Marcuson WF III (1978) Definition of terms related to liquefaction. J Geotech Geoenviron Eng 10(4):1197–1200
Maren A, Harston C, Pap R (1990) Handbook of neural computing applications. Academic press, San Diego
Moradi G, Khatiba BR, Sutubadi MH (2011) Determination of liquefaction potential of soil using (N1)60 by numerical modeling method. EJGE 16:407–417
Najjar YM, Ali HE (1999) Simulating the stress–strain behavior of Nevada sand byANN. In: Proceedings of the 5th U.S. national congress on computational mechanics (USACM), Boulder, Colorado
Najjar YM, Basheer IA, McReynolds R (1996) Neural modelling of Kansas soil swelling. Transportation research, record no. 1526, pp 14–19

Neaupane KM, Achet SH (2004) Use of backpropagation neural network for landslide monitoring: a case study in the higher Himalaya. Eng Geol 74:213–226

Orbanić P, Fajdiga M (2003) A neural network approach to describing the fretting fatigue in aluminum-steel couplings. Int J Fatigue 25:201–207

Ozer M, Isik NS, Orhan M (2008) Statistical and neural network assessment of the compression index of clay-bearing soils. Bull Eng Geol Environ 67:537–545

Park HI, Cho CH (2010) Neural network model for predicting the resistance of driven piles. Mar Georesour Geotech 28(4):324–344

Park HI, Kim YT (2010) Prediction of strength of reinforced lightweight soil using an artificial neural network. Eng Comput 28(5):600–605

Pathak SR, Dalvi AN (2011) Performance of empirical models for assessment of seismic soil liquefaction. Int J Earth Sci Eng 4:83–86

Penumadu D, Zhao R (1999) Triaxial compression behavior of sand and gravel using and artificial neural networks (ANN). Comput Geotech 24(3):207–230

Ramakrishnan D, Singh TN, Purwar N, Barde KS, Gulati A, Gupta S (2008) Artificial neural network and liquefaction susceptibility assessment: a case study using the 2001 Bhuj earthquake data, Gujarat, India. Comput Geosci 12:491–501

Rao KS, Satyam DN (2007) Liquefaction studies for seismic microzonation of Delhi region. Curr Sci India 92(5):646–654

Ripley BD (1996) Pattern recognition and neural networks. Cambridge University Press, Cambridge

Robertson PK, Campanella RG (1985) Liquefaction potential of sands using the CPT. J Geotechnical Eng 111(3):384–403

Robertson PK, Wride CE (1998) Evaluating cyclic liquefaction potential using the cone penetration test. Can Geotech J 35(3):442–459

Rumelhart DH, Hinton GE, Williams RJ (1986) Learning internal representation by error propagation. In: Rumelhart DE, McClelland JL (eds) Parallel distributed processing, Vol. 1, Chap. 8. MIT Press, Cambridge

Sakellariou MG, Ferentinou MD (2005) A study of slope stability prediction using neural networks. Geotech Geol Eng 23:419–445

Seed HB, De Alba P (1986) Use of SPT and CPT tests for evaluating the liquefaction resistance of sands. In: Proceedings of the In-situ, ASCE, New York, pp 281–302

Seed HB, Martin GR, Pyke CK (1978) Effects of multi-directional shaking on pore pressure development in sands. J Geotech Eng Div 104(1):27–44

Shahin MA, Jaksa MB (2005) Neural network prediction of pullout capacity of marquee ground anchors. Comput Geotech 32:153–163

Shahin MA, Jaksa MB, Maier HR (2001) Artificial neural network applications in geotechnical engineering. Aust Geomech 36(1):49–62

Shahin MA, Jaksa MB, Maier HR (2005). Stochastic simulation of settlement prediction of shallow foundations based on a deterministic artificial neural network model. In: Proceedings of the international congress on modelling and simulation, MODSIM 2005, Melbourne, Australia, pp 73–78

Shahin MA, Jaksa MB, Maier HR (2008) State of the art of artificial neural networks in geotechnical engineering. EJGE Special Volume Bouquet 08. http://www.ejge.com/Bouquet08/Shahin/Shahin_ppr.pdf

Shahin M, Maier H, Jaksa M (2002) Predicting settlement of shallow foundations using neural networks. J Geotech Geoenviron Eng 128(9):785–793

Shahin MA, Maier HR, Jaksa MB (2004) Data division for developing neural networks applied to geotechnical engineering. J Comput Civil Eng 18(2):105–114

Shi JJ (2000) Reduction prediction error by transforming input data for neural networks. J Comput Civil Eng 14(2):109–116

Shibata T, Teparaska W (1988) Evaluation of liquefaction potentials of soils using cone penetration tests. Soils Found 28(2):49–60

Singh TN, Gupta AR, Sain R (2006) A comparative analysis of cognitive systems for the prediction of drillability of rocks and wear factor. Geotech Geol Eng 24:299–312

Smith GN (1986) Probability and statistics in civil engineering: an introduction. Collins, London

Sonmez H, Gokceoglu C, Nefeslioglu HA, Kayabasi A (2005) Estimation of rock modulus: for intact rocks with an artificial neural network and for rock masses with a new empirical equation. Int J Rock Mech Min 43(2):224–235

Stark TD, Olson SM (1995) Liquefaction resistance using CPT and field case histories. J Geotech Eng 121(12):856–869

Thevanayagam S (2007a) Intergrain contact density indices of granular mixes-I: framework. J Earthq Eng Eng Vib 6(2):123–134

Thevanayagam S (2007b) Intergrain contact density indices of granular mixes-II: liquefaction resistance. J Earthq Eng Eng Vib 6(2):135–146

Thevanayagam S, Ecemis N (2008) Effects of permeability on liquefaction resistance and cone resistance. Geotech Earthq Eng Soil Dyn IV

Thevanayagam S, Kanagalingam T, Shenthan T (2003) Intergrain friction, contact density, and cyclic resistance of sands. In: Proceedings of the Pacific conference on earthquake engineering, University of Canterbury, Christchurch, New Zealand

Venkatesh K, Kumar V, Tiwari R (2013) Appraisal of liquefaction potential using neural networks and neuro fuzzy approach. Appl Artif Intel 27(8):700–720

Wang J, Rahman MS (1999) A neural network model for liquefaction-induced horizontal ground displacement. Soil Dyn Earthq Eng 18:555–568

Yoo C, Kim J-M (2007) Tunneling performance prediction using an integrated GIS and neural network. Comput Geotech 34:19–30

Young-Su K, Byung-Tak K (2006) Use of artificial neural networks in the prediction of liquefaction resistance of sands. J Geotech Geoenviron Eng 132(11):1502–1504

Zhao HB (2008) Slope reliability analysis using a support vector machine. Comput Geotech 35:459–467

Ziaie-Moayed R, Naeini SA, Baziar MH (2002) Evaluation of liquefaction potential of loose silty sand based on CPTU Results. In: Proceedings of Canadian geotechnical society conference, October 20–24, Canada, pp 95–100

Zurada JM (1992) Introduction to artificial neural systems. West, St. Paul